Electrostatically Enhanced Second and Third Virial Coefficients, Viscosity, and Interparticle Correlations for Linear Polyelectrolytes

Gina A. Sorci and Wayne F. Reed*

Physics Department, Tulane University, New Orleans, Louisiana 70118

Received December 3, 2001; Revised Manuscript Received April 2, 2002

ABSTRACT: The use of an automatic, continuous mixing (ACM) technique, coupled with multiangle static light scattering, refractometric, and viscometric detectors allowed detailed measurements of electrostatic effects in polyelectrolyte solutions to be made while varying ionic strength [I], and polyelectrolyte concentration. A linear polyelectrolyte, sodium hyaluronate (HA) was used. The behavior of second and third virial coefficients, A_2 and A_3, the angular scattering envelope, and the reduced viscosity were determined simultaneously. The crossover regime from where interparticle effects dominate the scattering to where single particle form factors dominate is clearly seen and is rationalized by a simple pair correlation function. Good agreement is found for polymer dimensions and A_2 using a combination of electrostatic persistence length and electrostatic excluded volume theories, with no adjustable parameters. The contribution to [I] from the HA counterions is observed via the electroviscous effect, a reduced viscosity crossover phenomenon, and an unusual scattering minimum vs polyelectolyte concentration at low [I].

Introduction

When the ionic strength [I] of a solution containing polyelectrolytes decreases, a number of effects are observed; the interparticle interactions, the polyelectrolyte static dimensions, and hydrodynamic radius all increase. At very low ionic strength, interparticle correlations can be strong enough that liquid-order type scattering maxima can be observed in concentrated solutions with X-rays and neutrons[1−4] and in dilute solutions with light,[5−9] including under flow conditions.[10] The so-called "electroviscous effect" has also been frequently documented in the low ionic strength regime.[11−13] At higher concentrations other effects, such as hydration forces, can dominate interparticle forces.[14−17] These phenomena continue to be a challenge to describe theoretically and are relevant in contexts such as control of solution viscosity, selective interactions, biological interactions, gelation, complexation, and other areas.

A review of electrostatic effects in polyelectrolytes is beyond the scope of this work, but a good summary of the current knowledge of polyelectrolyte solutions with extensive references is given by Forster and Schmidt.[18] The overall subject of excluded volume (EV) has been treated extensively by many authors. A good summary of approaches is in Yamakawa.[19] EV effects that are intramolecular cause polymer chain dimensions, e.g., as measured by root-mean-square radius of gyration $\langle S^2 \rangle^{1/2}$, to differ from their ideal values, whereas intermolecular EV effects can be measured by their influence on second, third and higher virial coefficients, A_2, A_3, etc.

The goal of the current work is to obtain extensive, continuous data on the behavior of electrostatically enhanced third virial coefficients A_3, (which is a measure of the three-body interactions, mediated by specific interparticle potentials) for which almost no data exist in the literature, and to obtain, simultaneously, data on A_2, (which is a measure of the two-body interaction) and polyelectrolyte static and hydrodynamic dimensions, the latter furnished via viscosity. Analysis using a combination of existing theories is made in order to understand the overall trends and relations between steric, hydrodynamic, and electrostatic excluded volume, and interparticle correlations. It is hoped that these data will be useful for more detailed theoretical studies, beyond the scope of this report, and that the automatic, continuous mixing technique presented here will prove valuable for other polyelectrolyte investigations.

Materials and Methods

Sodium hyaluronate (HA) was chosen as the linear polyelectrolyte for study. Its conformations and interactions have been successfully described using combined electrostatic and persistence length theories,[20] and it is hence a "well-behaved" polyelectrolyte. The HA used (Sigma, *Streptococcus zooepidemicus*) was exceptionally pure and yields no persistent aggregates when dissolved in aqueous solution of any ionic strength. A kinetic study yielding observations of the appearance and slow dissolution of polyelectrolyte aggregates in low ionic strength solution was recently reported[21] and lent further evidence to the notion that the frequently observed slow modes of diffusion or "extraordinary phase" of low ionic strength polyelectrolyte solutions[22,23] constitute a nonequilibrium aspect of such solutions.[24,25] In fact, the presence of such aggregates has been shown to mask the angular scattering maxima of solutions of well dispersed polyelectrolyte chains when the aggregates are not properly removed (e.g., by filtration or eventual dissolution).[6,9,26] This still contentious issue need not be addressed in this work, however, since no "slow modes" are observed at any ionic strength.

The mass of the dimeric repeat unit of HA is 400 g/mol, with a contour length of 10 Å. There is one elementary charge (COO^-) per repeat unit, giving a total of 0.7 charges per Bjerrum length λ_B ($\lambda_B = 7.18$ Å in pure water at $T = 25$ °C). Hence, HA is below the putative condensation threshold,[27] and so counterion condensation effects need not be considered. HA has not previously shown an $I(q)$ maximum at low salt by light scattering,[20] although such maxima have been found for many other polyelectrolytes. New work by Villetti et al. at high concentrations shows an $I(q)$ maximum using high flux synchrotron X-rays.[28]

Gel permeation chromatography (GPC) was used to assess the polydispersity of the HA; $M_z/M_w = 1.5$, and $M_w/M_n = 3.0$.

* Corresponding author.

10.1021/ma012103n CCC: $22.00
Published on Web 05/15/2002

The apparatus consisted of a Hewlett-Packard 1100 isocratic pump, Shodex QB804 and QB806 columns in series, an Anspec RI detector, and a home-built, seven-angle laser light scattering detector, previously described.[29,30]

In the ACM experiments the HA and/or NaCl were dissolved in deionized water (0.5 μmohm) which was filtered with 0.1 μm filter previous to HA dissolution. After the sample was completely dissolved, it was filtered using a 0.45 μm Millipore filter. The samples were then primed in the lines of an Isco 2360 programmable gradient mixer. This was connected to an Isco 2350 pump. In line following the pump there was a 1 cm diameter filter with a 0.5 μm frit and a 25 mm filter with 10 μm frit both from Upchurch and inside of the 25 mm filter there was a 0.22 μm Millipore paper filter. Next was a Wyatt corporation Dawn DSP 18 angle light-scattering detector in flow mode, a home-built capillary viscometer, and a Waters 2410 refractometer (RI). The data were collected and analyzed with a computer using software developed by the authors.

The time response and repeatability of the system has been previously reported.[31] In that work, concentration ramps were carried out from low to high solute and then back from low to high to ensure the data overlapped.

The usual Zimm approximation for the excess Rayleigh scattering ratio $I(c,q)$ is the starting point for most of the light scattering analysis[32]

$$\frac{Kc}{I(c,q)} = \frac{1}{MP(q)} + 2A_2c + [3A_3Q(q) - 4A_2^2MP(q)(1 - P(q))]c^2 + O(c^3) \quad (1)$$

where c is the polymer concentration (g/cm^3), $P(q)$ is the particle form factor, q is the amplitude of the scattering wave vector $\mathbf{q} = (4\pi n/\lambda)\sin(\theta/2)$, where θ is the scattering angle and K is an optical constant, given for vertically polarized incident light by

$$K = \frac{4\pi^2 n^2 (\partial n/\partial c)^2}{N_A \lambda^4} \quad (2)$$

where n is the solvent index of refraction, λ is the vacuum wavelength of the incident light, N_A is Avogadro's number, and $\partial n/\partial c$ is the differential refractive index for the polymer in the solvent. $Q(q)$ involves a sum of complicated Fourier transforms of the segment interactions that define A_2. In the limit of $q = 0$, $P(0) = Q(0) = 1$, so that, for a polydisperse polymer population, this becomes

$$\frac{Kc}{I(c,0)} = \frac{1}{M_w} + 2A_2c + 3A_3c^2 + O(c^3) \quad (3)$$

For low enough concentrations such that the c^2 term in eq 1 is negligible, and for $q^2\langle S^2\rangle_z < 1$, another, frequently used form of the Zimm equation is

$$\frac{Kc}{I(c,q)} = \frac{1}{M_w}\left(1 + \frac{q^2\langle S^2\rangle_z}{3}\right) + 2A_2c \quad (4)$$

As pointed out in other polyelectrolyte studies,[20,33] in this limit $\langle S^2\rangle_z$ can be determined at low concentrations if M_w is known, without a full extrapolation to $c = 0$, and that a useful asymptotic form for ideal coils yields a polydispersity-independent value.[20] $\langle S^2\rangle_z^{1/2}$ is the z-average mean square radius of gyration. Throughout this work, whenever a model is employed, the experimental values of $\langle S^2\rangle_z$ will be used, even when the model is based on the monodisperse value of $\langle S^2\rangle$.

The value $\partial n/\partial c = 0.155$ for HA was used. There is considerable variation of $\partial n/\partial c$ in the literature, ranging from 0.138 to 0.20.[34] In principle, $\partial n/\partial c$ is the value used when the polyelectrolyte is in dialysis equilibrium with the aqueous solvent of given ionic strength.[35,36] Work that is currently underway shows this effect to be small regardless of the salt used.

The voltage $V(t)$ of the single capillary viscometer is directly proportional to the total viscosity of the solution flowing through the capillary. This allows the reduced viscosity η_r to be computed at each instant, without any calibration factor, according to

$$\eta_r(t) = \frac{V(t) - V(0)}{V(0)c(t)} \quad (5)$$

where $V(0)$ is the viscometer voltage when pure solvent flows. The intrinsic viscosity $[\eta]$ is related to η_r according to

$$\eta_r = [\eta] + \kappa_{H1}[\eta]^2c_p + \kappa_{H,2}c_p^2 + O(c_p^3) \quad (6)$$

where κ_{H1} is $\sim$0.4 for neutral polymers.[37] Unfortunately, no theoretical forms for $\kappa_{H,2}$ random coils exist, although empirical forms exist.[38] For hard spheres $\kappa_{H,2} = \kappa_{H,2}^2$. $[\eta]$ measures the hydrodynamic volume V_H, per unit mass according to

$$[\eta] = \frac{5V_H}{2M}N_A \quad (7)$$

Shear rates in the capillary viscometer were on the order of 500 s^{-1}.

Results and Discussion

Figure 1a shows raw viscosity, RI, and light-scattering data (at $\theta = 90°$) data vs time for HA at 0.1 mg/mL with an NaCl concentration ramp, spanning 0−0.4 M. The first portion, to about 500 s, shows the baselines of each instrument stabilized with pure water. A large increase in viscosity is seen when 0.0001 g/mL HA is pumped through in pure water, but only a small increase in light scattering occurs. At about 2500 s the NaCl ramp begins over the regime [NaCl] = 0−0.01 M. Subsequently, the discontinuities are due to changing ionic strength reservoirs at different times. The first ramp lasted 120 min. However, at about 6000 s, the [NaCl] was abruptly increased to 0.01 M, held there for about 2000 s, and then slightly decreased and allowed to rise back again to 0.10 M. This demonstrates the rapid reversible response of both the light-scattering and viscosity signals to rapid changes in [NaCl]. This period was followed by two 60 min ramps. The first reservoir allowed the ramp to go from 0.01 to 0.1 M NaCl, and the third from 0.1 to 0.4 M NaCl. Here, 0.4 M NaCl is the highest value obtainable before saturating the RI on its least sensitive scale. The reservoir changes were done because the effect of [NaCl] on scattering and viscosity increases in roughly logarithmic fashion, so that more sampling per moles per liter of NaCl should be done in the lower [NaCl] range. More sophisticated pumps than that used here allow gradient profiles to be programmed, so that a single reservoir could be used.

Figure 1b shows the raw data vs [NaCl] for the same data as Figure 1a, where [NaCl] was determined from the RI data and dn/dc = 0.174 for NaCl.[39] It should be noted that the discontinuities seen from the reservoir changes in Figure 1a disappear when the data is plotted vs [NaCl], including the abrupt changes. The expected trends vs [NaCl] are clearly seen: Scattering intensity increases with increasing [NaCl], due to the decrease in interchain repulsion and decrease in the virial coefficients. Viscosity decreases as the polymer coil contracts due to screening, giving a smaller hydrodynamic volume, and hence smaller intrinsic viscosity.

Figure 2 shows the $q = 0$ intercepts of $Kc/I(c,q)$ vs [NaCl] for HA at 0.1 and 1 mg/mL. The intercept was

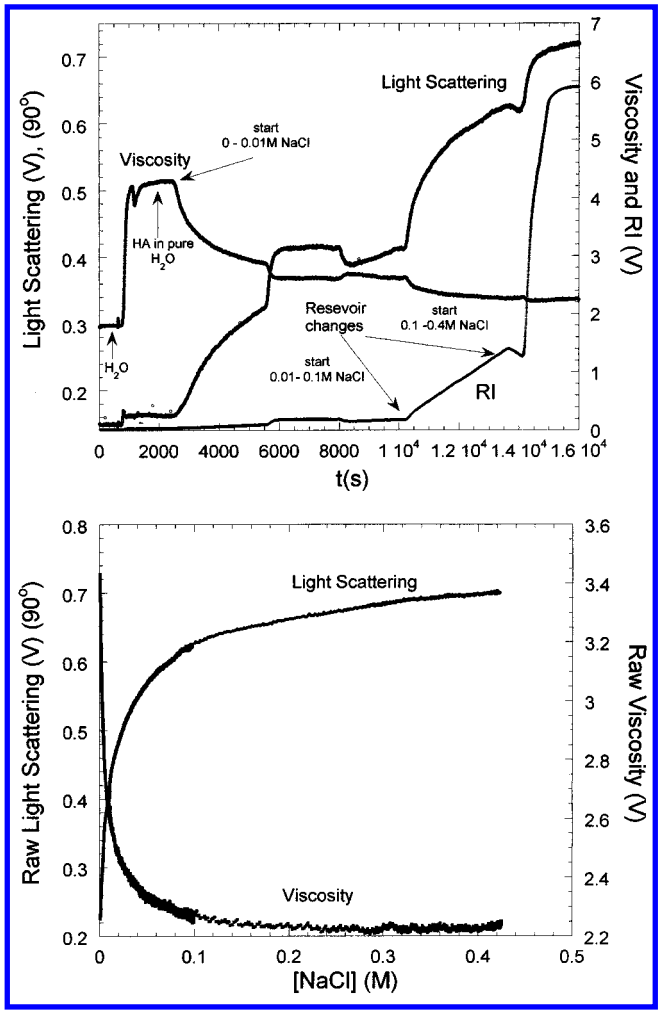

Figure 1. (a) Raw light-scattering, viscosity and RI data vs time for a typical ramp of [NaCl] with fixed c (0.1 mg/mL). NaCl reservoir changes are shown. (b) With RI data from Figure 1a, light-scattering and viscosity data represented vs [NaCl]. Notice that the significant discontinuities from the reservoir changes in Figure 1a are no longer apparent in this representation.

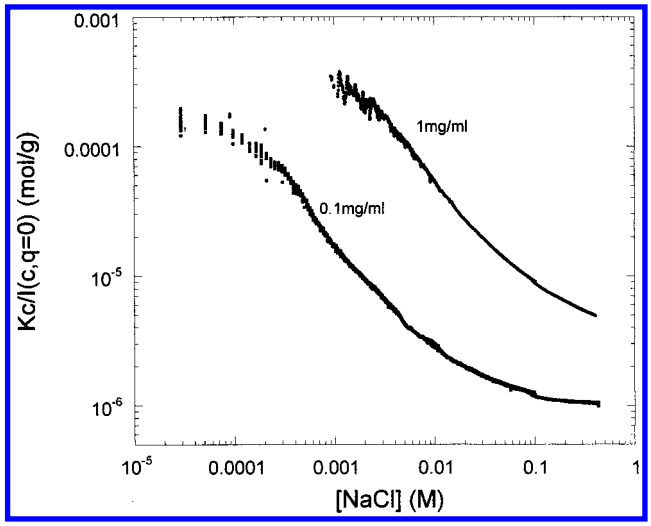

Figure 2. Enormous effect of ionic strength on light scattering shown by the $q = 0$ light-scattering intercept, represented as $Kc/I(c,q = 0)$ vs [NaCl] for $c = 0.0001$ g/mL and $c = 0.001$ g/mL.

found from linear extrapolation of $Kc/I(q,c)$ vs q^2 over the range 25−141°. The steep drop with increasing salt reflects the interparticle shielding and decrease in A_2 and A_3. The higher values of $Kc/I(0,c)$ for higher c follow directly from the $2A_2c$ and $3A_3c^2$ terms in eq 3. A_2 and A_3 are extracted from these and similar data below.

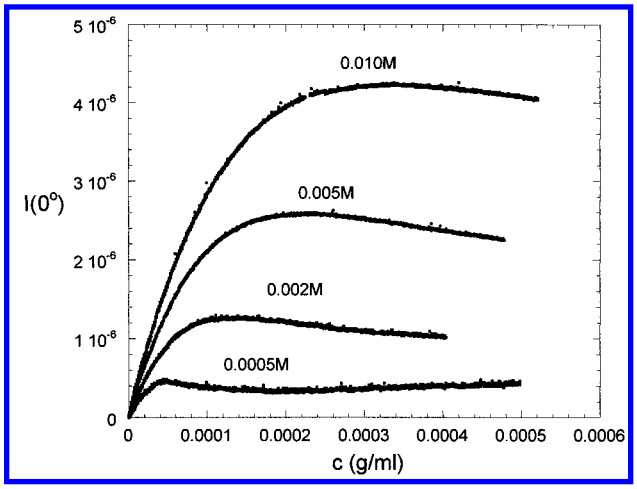

Figure 3. Raw light-scattering data (at $\theta = 90°$) vs c, at several fixed values of [NaCl]. The maximum in each is due to the electrostatically enhanced A_3, as described in the text.

Figure 3 shows strong polyelectrolyte behavior when [NaCl] is held constant and c increases. The absolute scattered intensity $I(c,q(90°))$ vs c for several fixed values of [NaCl] is shown, and the scattered intensity at a given value of c increases dramatically with increasing [NaCl], in agreement with Figure 1b. A maximum in scattered intensity is reached as c increases. This is due to the effect of A_3. Using the $q = 0$ extrapolations of the scattered intensity allows A_3 to be found from the $q = 0$ limit of the Zimm approximation, eq 3, according to

$$A_3 = \frac{1}{3M_w c_m(q=0)^2} \tag{8}$$

where $c_m(q = 0)$ is the position of the scattering maximum at $q = 0$. $c_m(q)$ decreases monotonically with q, and is related to the complex factor $Q(q)$ in eq 1. The lower value of c_m with decreasing [NaCl] is due to the increase of A_3 with decreasing ionic strength.

The behavior of the scattered intensity at 0.0005 M [NaCl] reveals a minimum in the scattering after the maximum. This may be due to the contribution of the HA counterions to ionic strength, much as it is believed to occur in the electroviscous effect. These points are discussed below.

Figure 4a shows A_2 vs [NaCl], obtained from Figure 2 data and other, related data. A_2 and A_3 (Figure 4b) were calculated using a convergent, iterative method, as follows. The intercept values $Kc/I(c,q = 0)$ were taken from an experiment at low c (0.0001 g/mL in this case) in which the [NaCl] was ramped 0−0.4 M, and A_2 was found from eq 3, assuming $A_3 = 0$, and using the experimental value of $M_w = 1.5 \times 10^6$ g/mol. Then, $Kc/I(c,q = 0)$ from a much higher fixed HA concentration (0.001 g/mL, with the same 0−0.4 M NaCl ramp) was used with eq 3, using the values of A_2 computed at low concentration. To apply this procedure, a program was written to match the [NaCl] values for the two experiments. These initial values of A_2 and A_3 are shown in Figure 4, parts a and b, respectively. The values of A_3 were then substituted back into eq 3 using the low c data for $Kc/I(c,q = 0)$, yielding a first correction to A_2.

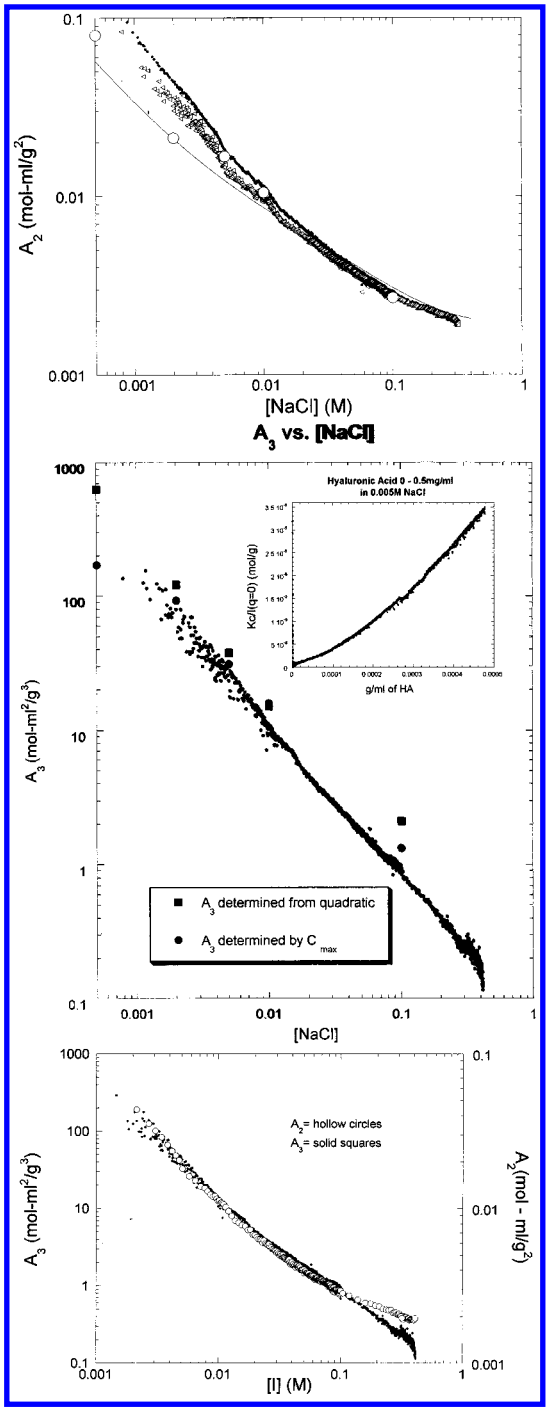

Figure 4. (a) Continuous record of A_2 determined from data at $c = 0.0001$ g/mL, such as in Figure 3, according to methods explained in the text. The large, hollow circles were obtained from linear fits to $Kc/I(c = 0,q)$ at low c, at fixed values of [NaCl], using eq 3. The top record (solid circles) corresponds to the first approximation to A_2, and the line below it (hollow triangles) is from the convergent, iterative method involving A_3 and a second experiment at $c = 0.001$ g/mL. The solid line is a computation involving combined EEV and EPL theories, described in the text, and involves no adjustable parameters. (b) Continuous record of A_3 obtained from a ramp of [NaCl] at $c = 0.001$ g/mL, in conjunction with the values of A_2 in Figure 4a. The squares are values obtained from quadratic fits to $Kc/I(c,q = 0)$ in eq 3 at fixed [NaCl]. The circles are values obtained using the maxima in light scattering vs c, at $q = 0$, in conjunction with eq 8. The inset shows an example of $Kc/I(c,q = 0)$ vs c, used for quadratic fitting in eq 3. (c) A_2 and A_3 from parts a and b plotted vs [I], using eq 10. This shows A_3 proportional to A_2^2 over most of the range of [I].

As expected, these values are somewhat lower than the starting values when $A_3 = 0$ was assumed, the difference being most pronounced at low [NaCl]. These corrected A_2 values were then used to re-compute A_3, and so on. The first iteration values of A_2 are also shown in Figure 4a. Successive iterations produced no significant further changes in A_2. In Figure 4b only the initial values of A_3 are shown, because even the first iteration was only negligibly different than the starting values.

Also shown in Figure 4a are the values of A_2 determined by linear fits of $Kc/I(c,q = 0)$ at very low values of c, at fixed values of [NaCl]. These values lie very close to the continuous A_2 values determined by iteration of the experiments at high and low values of c. The solid line in Figure 4a is a computation using combined EPL and EEV, and is discussed below.

In Figure 4b the squares are the values of A_3 obtained from a quadratic fit to eq 3 for $Kc/I(c,q = 0)$ at higher values of c. The inset to Figure 4b shows an example of $Kc/I(c,q = 0)$, where its pronounced quadratic nature is clear. This behavior again shows how electrostatic effects overwhelmingly control the scattering intensity via the A_2 and A_3 terms. The circles in Figure 4b correspond to the determination of A_3 via eq 8 above, using the values of c where the maxima occur at $q = 0$. To obtain these latter, $I(c,q = 0)$ was computed from the values of $Kc/I(c,q = 0)$, and the maxima in $I(c,q = 0)$ found.

There is no single power law that expresses the dependence of A_2 on [NaCl]. Over the range 0.001 M to 0.01 M [NaCl] there is a fairly well-defined 1/[NaCl] dependence, which becomes closer to $1/[\mathrm{NaCl}]^{0.5}$ in the 0.01−0.1 M range, after which A_2 appears to approach an asymptotic value close to 0.002. This suggests that there is no value of [NaCl] at $T = 25$ °C that will yield a Θ condition (i.e., at which $A_2 = 0$) for HA. This is in contrast to results for PSS,[40] for example, for which a putative Θ condition was found at high [NaCl], via extrapolation (at $T = 25$ °C). This may be related to the fact that PSS has a much smaller intrinsic persistence length, around 1 nm, in contrast to HA which is around 10 nm. The impressive span of A_2 of 2 orders of magnitude going from 0.001 to 0.4 mM [NaCl] shows the predominance of the electrostatic portion of A_2, whereas the limiting value of $A_2 = 0.002$ at high salt shows the residual "neutral polymer" type random coil contribution to A_2.

The simplest possible approach to interpreting A_2 is that for ideal polyelectrolytes, for which considerations of Donnan equilibrium and electroneutrality yield a "Donnan A_2", corresponding to the quadratic polymer concentration term in the osmotic pressure expansion, given by

$$A_{2,\mathrm{Donnan}} = \frac{Z_{\mathrm{eff}}^{\,2}}{4C_s M_n^{\,2}} \qquad (9)$$

In fact, the approximate 1/[NaCl] power law in the 0.001−0.01 M regime obeys this, and, surprisingly, the value of Z_{eff} computed, using the GPC value of $M_n = 5 \times 10^5$ g/mol, is $Z_{\mathrm{eff}} = 390$, which is at least on the same order of magnitude of $Z = 1250$ obtained from purely stoichiometric considerations. Effective values of Z, for example those found by dynamic light scattering, are often found to be a small fraction of the stoichiometric charge.[22,23] We do not expect, however, that such a facile

model as ideal Donnan equilibrium can well describe a polyelectrolyte with a large, salt-sensitive random-coil type spatial structure. In fact, as pointed out long ago by Scatchard et al.[41] the Donnan and electroneutrality conditions yield $A_3 = 0$. Figure 4b shows that A_3 is very large and can completely dominate scattering. Hence, not surprisingly, while the simple Donnan picture gives a fair order of magnitude estimate for Z_{eff}, it fails to provide a picture for the large A_3.

The values of A_3, in fact, are remarkably and consistently proportional to A_2^2, over the range 0.001−0.2 M, as seen in Figure 4c. In Figure 4c the estimated contribution of the HA counterions to [I] (in molar units) was computed via

$$[\mathrm{I}] = [\mathrm{NaCl}] + \beta c \tag{10}$$

where $\beta = 1.25$ M/(g/mL) for HA assumes that only the HA Na^+ counterions contribute to [I]. This is discussed further below.

The simplest available model for A_3 is that of hard spheres, for which[42]

$$A_3 = \epsilon\frac{5MA_2^2}{8} \tag{11}$$

where $\epsilon = 1$ for hard spheres. For neutral polymers that resemble random coils, ϵ is usually found experimentally to range from 0.25 to 0.75,[43−45] A lattice-model Monte Carlo study concludes that $\epsilon = 0.481$, universally, for long chain, neutral polymers.[46] Values of ϵ were found to range from 0.15 to 0.70 for pseudopolyelectrolytes formed by the association between neutral PVP and SDS micelles.[31] From Figure 4c the value is about 0.1 over the range of nearly constant ϵ. Nordmeier[40] found a similar constancy of $\epsilon \sim 0.1$over the range [NaCl] = 5−100 mM for PSS, with a very large increase to over 2 by 1000 mM.

It is truly remarkable that the hard sphere scaling between A_2 and A_3 holds over such a wide range of ionic strengths for particles interacting via a "soft", screened Coulombic potential. This allows the interactions to be modeled, at least in some contexts, as spheres of an effective equivalent volume of exclusion, which is significantly larger than the "hard" portion of the polymer coils.

Figure 5a shows $Kc/I(q,c)$ vs q^2 for 0.1 mg/mL HA at different [NaCl]. At low [NaCl], the slope is *negative*, indicating strong interparticle correlations. As [NaCl] increases, the slope becomes positive, and it remains positive but with decreasing slope as [NaCl] continues to increase.

Figure 5b shows the slope $\mathrm{d}[Kc/I(q,c)]/\mathrm{d}q^2$ vs c for different [NaCl]. The slope decreases strongly with c at low [NaCl] but is virtually independent of c at [NaCl] = 0.1 M. In all cases, there is a plateau of slope over some region of low c, the height of which decreases with increasing [NaCl]. The dependence of the slope on c is also a result of strong interparticle effects. At sufficiently low ionic strength, e.g., 2 mM, the slope becomes negative. Negative slopes of this type were previously reported for proteoglycan subunits[6] and occurred for concentrations higher than those that yielded scattering maxima within the range of q available to the scattering experiments. Figure 5a shows the first reported evidence of a negative slope in light scattering for HA, all previous attempts having failed to find either a negative slope or a q-dependent scattering maximum.

Over the plateau region the interparticle effects are suppressed sufficiently that the only source of the slope is $\langle S^2\rangle_z$ in eq 4. The asymptotic form of $P(q)$ for ideal, polydisperse random coils[47] has been used in this limit in earlier work.[20,33] Here, we simply use eq 4 to estimate $\langle S^2\rangle_z$ and do not use the asymptotic form or make any corrections for polydispersity.

Figure 5c shows the slope vs [NaCl]. As [NaCl] decreases, the slope increases, which, again, is a direct measure of $\langle S^2\rangle_z$ according to eq 4, as long as there is no strong interparticle spatial correlation. The build-in of strong interparticle correlations can be seen at lower [NaCl], where the slope first reaches a maximum, then decreases, eventually becoming negative. Consistent with Figure 5b, the concentration of [NaCl] at which the maximum in the slope occurs decreases as c decreases. The values of the slope converge well at higher [NaCl] where the correlations are suppressed. Also shown on the figure are large, hollow squares, corresponding to the $c = 0$ values of the slopes from Figure 5b. They are in excellent agreement with the slope values vs [NaCl] obtained at $c = 0.04$ mg/mL. This confirms the procedure used here, and previously,[20,33] which bases finding $\langle S^2\rangle_z$ on single measurements of the slope at finite c.

A starting point for modeling competing intra- and interparticle effects is to use the often evoked relation between excess scattering $I(q,c)$ and the single particle form factor $P(q)$, and the interparticle structure factor $S(q)$

$$\frac{I(c,q)}{K} = McS(q)P(q) \tag{12}$$

where

$$S(q) = 1 + N\int[g(\vec{\mathrm{r}}) - 1]e^{i\vec{\mathrm{q}}\cdot\vec{\mathrm{r}}}\,\mathrm{d}^3r \tag{13}$$

and $\vec{r}$ is the interparticle displacement vector, N is the particle density (particles/mL), and $g(\vec{r})$ is the interparticle correlation function given by

$$g(\vec{r}) = \exp\left(-\frac{U(\vec{r})}{k_\mathrm{B}T}\right) \tag{14}$$

where $U(\vec{r})$ is the interparticle potential energy and k_B is Boltzmann's constant. For central forces between particles, i.e., for those which depend only on the interparticle separation r, eq 13 can be integrated over azimuth and altitude angles to yield

$$S(q) = 1 + \frac{4\pi N}{q}\int_0^\infty[g(r) - 1]r\,\sin(qr)\,\mathrm{d}r \tag{15}$$

$S(q)$ has been computed for several models of $U(r)$, including hard sphere,[48] Debye screening of a point charge,[49] and a quasi-periodic damped potential.[26] In the simplest model of the hard sphere, the coil-type polyelectrolyte is imagined to have an equivalent, spherically symmetric radius of exclusion around itself R due cheifly to the screened Coulombic interactions. This model, the equivalent hard sphere, provides the most uncluttered ansatz for analyzing the slope behavior. Its use is supported by the remarkable result in

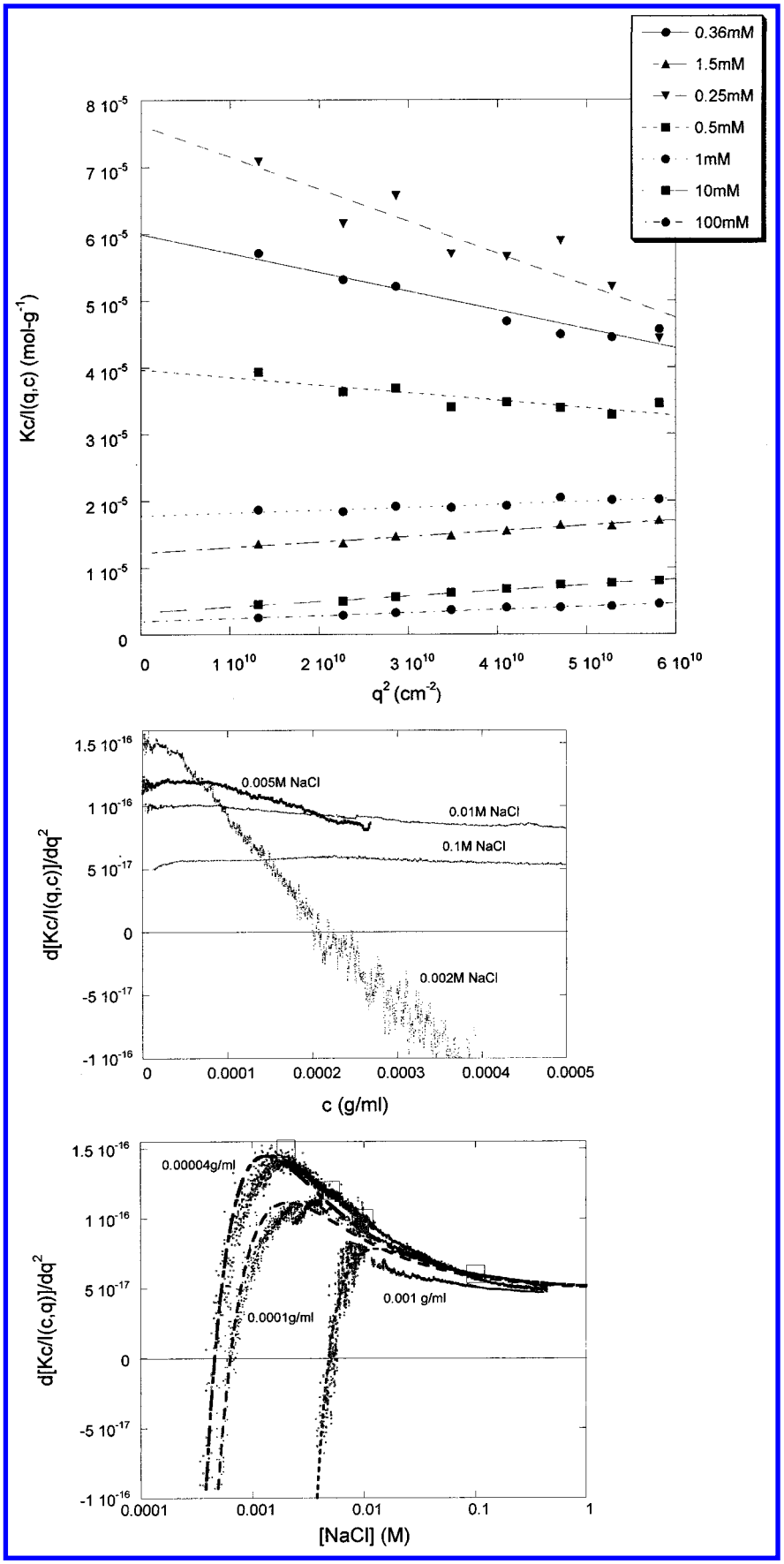

Figure 5. (a) Selected plots of $Kc/I(q,c)$ vs q^2 for 0.1 mg/mL HA at different [NaCl]. (b) Slope $d[Kc/I(q,c)]/dq^2$ vs c for fixed values of [NaCl], as obtained from data such as in Figure 1b. The origin of the negative slopes at low [NaCl] are discussed in the text. (c) Slope $d[Kc/I(q,c)]/dq^2$ vs [NaCl] for fixed c. The white squares are slopes obtained by extrapolation to $c = 0$ at fixed [NaCl]. The dashed lines are fits using the correlation model eq 18.

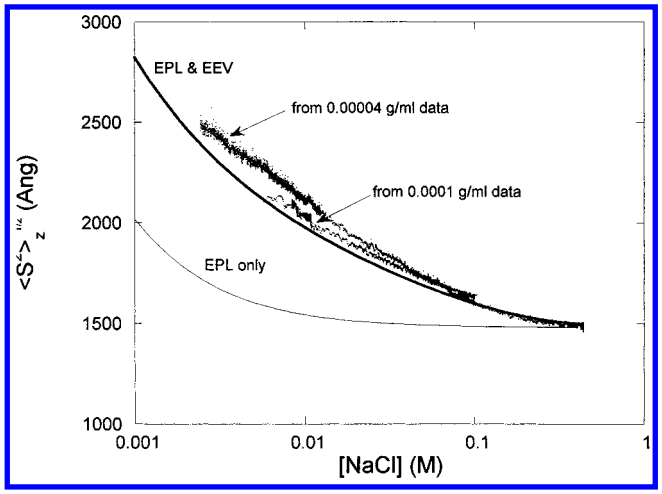

Figure 6. $\langle S^2\rangle_z^{1/2}$ vs [NaCl] obtained from the 0.00004 and 0.0001 g/mL data in the regime where interparticle effects are suppressed. The top solid line is the computation (not a fit) of $\langle S^2\rangle_z^{1/2}$ according to the combination of EPL and EEV theories outlined in the text. The lower line is the computation based only on the EPL effect.

Figure 4c that A_3 scales with A_2^2 at low ionic strength in accord with an equivalent hard sphere. $S(q)$ has the form

$$S(q) = 1 - 32\pi NR^3\left[\frac{\sin(x) - x\cos(x)}{x^3}\right] \qquad (16)$$

where $x = 2qR$. Expanding $S(q)$ and $P(q)$ [$P(q) = 1 - q^2\langle S^2\rangle/3 + O(q^4)$], and retaining only terms of order q^2 yields (ignoring polydispersity)

$$\frac{KcM}{I(q,c)} = \left(1 + \frac{32\pi NR^3}{3}\right) + q^2\left[\frac{\langle S^2\rangle}{3} - N\left(\frac{32\pi\langle S^2\rangle R^3}{9} + \frac{64\pi R^5}{15}\right)\right] \qquad (17)$$

Hence, the slope is

$$\frac{d\left[\frac{Kc}{I(q,c)}\right]}{dq^2} = \frac{\langle S^2\rangle}{3M} - \frac{N}{M}\left(\frac{32\pi\langle S^2\rangle R^3}{9} + \frac{64\pi R^5}{15}\right) \qquad (18)$$

which yields a simple model for how the slope linearly decreases, and becomes negative with increasing particle density N. After the plateaus in Figure 5b, the decrease in slope in each case is well approximated by a linear fit. Again in the theoretical equation $\langle S^2\rangle$ bears no subscript, whereas, when experimental data are used, $\langle S^2\rangle_z$ is employed.

Using the portion of the data where interparticle correlations are small or negligible, Figure 6 shows $\langle S^2\rangle_z^{1/2}$ vs [NaCl], for data with $c = 0.00004$ and 0.0001 g/mL. These values were obtained from eq 4 using $M_w = 1.5 \times 10^6$ g/mol. The expected effect of decreasing $\langle S^2\rangle_z$ with increasing [NaCl] is clear. While there is no reason to expect an unambiguous power law for $\langle S^2\rangle_z$, a direct power law fit yields

$$\langle S^2\rangle_z(\text{Å}^2) = 1.255 \times 10^5[\text{NaCl}]^{-0.609} + 2.19 \times 10^6 \qquad (19)$$

where the value of 2.19×10^6 is $\langle S^2\rangle_z$ extrapolated to high [NaCl]. Using an assumed, [NaCl] dependent correlation between $\langle S^2\rangle^{1/2}$ and the effective radius R, of the type

$$\langle S^2\rangle^{1/2} = a[\text{NaCl}]^b R \qquad (20)$$

in eq 18, with the two parameters a and b, produces the fits shown by the dashed lines in Figure 5c. These are in good agreement with the experimental slopes, lending support to the basic idea for the factors governing the slope just explained.

The wormlike chain expression for a random coil with no excluded volume is[50]

$$\langle S^2\rangle_0 = \frac{LL_p}{3} - L_p^2 + 2L_p^3/L - 2\left(\frac{L_p^4}{L^2}\right)[1 - \exp(-L/L_p)] \qquad (21)$$

where L is the contour length of the polymer and L_p the persistence length. The measured $\langle S^2\rangle$ for a polyelectrolyte is larger than $\langle S^2\rangle_0$, due to electrostatic excluded volume effects, but these effects cannot be distinguished from local stiffening effects experimentally. Hence, in earlier works, $\langle S^2\rangle_0$ was replaced by $\langle S^2\rangle$, and the resulting persistence length obtained from eq 21 was termed the "apparent persistence length", L_p'. The extrapolation of $\langle S^2\rangle_z$ to infinite salt yields an apparent intrinsic persistence length of $L_{T,o}' = 175$ Å. In eq 21, L is the contour length of the polymer, which for HA can be computed from Nb, where $b = 1$ Å/40 g × mol^{-1}, and N is the number of links in the polymer. No correction has been made for polydispersity. The empirical scaling law of $[\text{NaCl}]^{-0.6}$ is close to the approximate -0.5 exponent found in other works,[20,51−53] including Monte Carlo calculations.[54]

Figure 6 also includes a computation of $\langle S^2\rangle^{1/2}$ based on a combination of electrostatic persistence length (EPL) and electrostatic excluded volume (EEV) theories used previously. The computation contains no adjustable parameters and is hence *not a fit to the data.* It requires the following experimentally or chemically known parameters: the apparent persistence length at extremely high ionic strength (175A), the mass of the polymer (1.5×10^6), the contour length per monomer (10A), the mass per monomer (400 g × M^{-1}), the dielectric constant of the medium (78.3), the chain diameter (10 Å), and the number of elementary charges per Bjerrum length (0.7). The agreement between the computation and the data is reasonably good. $\langle S^2\rangle$ is computed by a procedure previously summarized.[55] Namely, following Odijk[56] and Skolnick and Fixman,[57] it is assumed that at any value of ionic strength the total persistence length is the sum of the intrinsic persistence length $L_{p,0}$ and an electrostatic contribution given by the EPL, or L_e, where L_e is normally a small perturbation to $L_{p,0}$. That is $L_p = L_{p,0} + L_e$, and L_e was computed to be

$$L_e = \frac{\xi^2\kappa^{-2}}{12\lambda_B}\left[3 - \frac{8}{y} + e^{-y}\left(y + 5 + \frac{8}{y}\right)\right] \qquad (22)$$

where ξ is the number of elementary charges per Bjerrum length, κ is the Debye−Hückel screening parameter, and $y = \kappa L$. With knowledge of $L_{p,0}$ obtained at very high ionic strength, L_p can hence be computed using $L_{p,0}$ and L_e from eq 22, so that $\langle S^2\rangle_0$ can be computed by eq 21. The measured value $\langle S^2\rangle$ is related to $\langle S^2\rangle_0$ via the static expansion factor α_s

$$\langle S^2\rangle = \alpha_s^{\,2}\langle S^2\rangle_0 \tag{23}$$

There are several theories that relate α_s to the usual perturbation parameter z, given by

$$z = \left(\frac{3}{2\pi L_k^{\,2}}\right)\beta N_k^{\,1/2} \tag{24}$$

where L_k and N_k are the (Kuhn) statistical segment length and number, respectively, and $L_k = 2L_p$ in the coil limit. Here β is the excluded volume between two charged rodlike segments, for which Fixman and Skolnick arrived at the expression

$$\beta = 8L_p^{\,2}\kappa^{-1}\int_0^{\pi/2}\sin^2\theta\int_0^{w/\sin\theta}x^{-1}(1-e^{-x})\,dx\,d\theta \tag{25}$$

where

$$w = 2\pi\xi^2\kappa^{-1}e^{-\kappa d} \tag{26}$$

where d is the rod diameter.

Of the several expressions relating z to α_s one that has found considerable utility when $N_k > 2$, is the Gupta−Forsman expression[58]

$$\alpha_s^{\,5} - \alpha_s^{\,3} \approx \frac{134}{105}(1 - 0.885N_k^{\,-0.462})z \tag{27}$$

Figure 6 shows that the EEV effect dominates over the EPL effect, and, in fact, if only EPL effect is considered, the computation severely underestimates $\langle S^2\rangle_z^{1/2}$. Another case where EEV effects were dominant compared to EPL was demonstrated by Beer et al.[59] They found good agreement between the experimental values of $\langle S^2\rangle^{1/2}$ with theories based largely on the results of Muthukumar[60,61] for cationic hydrophobically modified poly(vinylpuridinium).

Figure 4a shows the results of an EEV/EPL computation for A_2 (solid line), as was carried out for $\langle S^2\rangle$. This computation builds off the procedure summarized above, where the Yamakawa expression for A_2 is used

$$A_2 = \left(\frac{N_A N_k^{\,2}\beta}{2M^2}\right)h_0(\bar{z}) \tag{28}$$

where

$$h_0(\bar{z}) = \frac{1-(1+3.9\bar{z})^{-0.468}}{1.83\bar{z}} \tag{29}$$

and $\bar{z} = z/\alpha_s^3$ is Yamakawa's first-order attempt at including intramolecular excluded volume into the intermolecular excluded volume problem. The agreement is best at higher [NaCl].

Figure 7 shows reduced viscosity vs [NaCl] for different HA at 0.001 and 0.0001 g/mL. The hydrodynamic volume of the HA coils decreases with increasing [NaCl], leading to the viscosity decrease. An interesting feature is the crossover of η_r at 0.0018 M NaCl. At [NaCl] lower than this value, the less concentrated solution actually has a larger value of η_r. This is believed to be due to the greater contribution of the HA counterions to the total solution ionic strength for the more concentrated solution. This is discussed below.

Figure 8 shows η_r vs c at [NaCl] = 0.005 and 0.1 M. A normal viscosity dependence is found according to eq 6, which is in agreement with the differences in η_r for HA in the main part of the figure. κ_{H1} decreases with decreasing [NaCl], and has the values 0.24, 0.1, and 0.04 at [NaCl] = 0.1, 0.01, and 0.005 M, respectively.

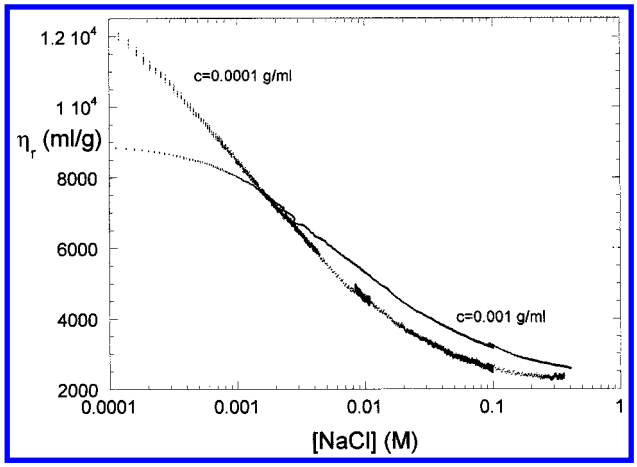

Figure 7. η_r vs [NaCl] for c = 0.0001 and c = 0.001 g/mL. The crossover is due to the contribution of the HA counterions to total solution ionic strength.

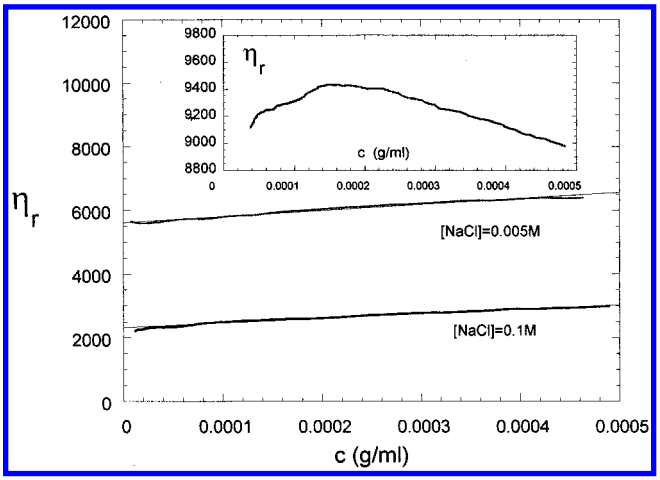

Figure 8. η_r vs c for [NaCl] = 0.005 and 0.1 M. The inset shows the electroviscous effect for HA at [NaCl] = 0.0005 M.

The inset to Figure 8 shows the electroviscous effect for HA at [NaCl] = 0.0005 M. It consists of an increase in η_r as c decreases, followed by a maximum, and subsequent decrease as c decreases further. It is discussed below in terms of the contribution of the HA counterions to total solution ionic strength.

The viscosity data here could be useful in achieving control of viscosity behavior. For example, combining the c and [NaCl] behaviors allows iso-viscosity paths in the c−[NaCl] plane to be predicted. [η] vs [NaCl] closely obeys the relation

$$[\eta] = -223 - 2770\log[\mathrm{NaCl(M)}] \tag{30}$$

Combining this with the usual form for total solution viscosity to second order in c

$$\eta = \eta_0(1 + [\eta]c + \kappa_{H1}[\eta]^2c^2 + O(c^3)) \tag{31}$$

allows the following equation for isoviscosity curves in the c/[NaCl] plane to be expressed

$$c = \frac{(1+4\eta_{rel})^{1/2} - 1}{2\kappa_{H1}[\eta]} \tag{32}$$

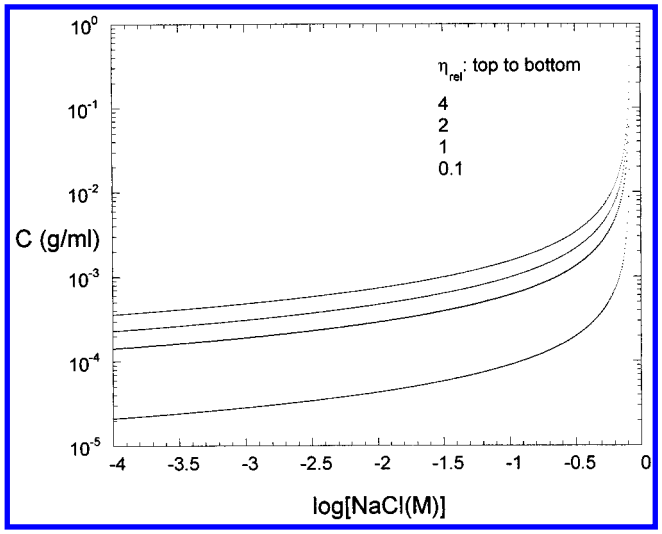

Figure 9. Isoviscosity curves for HA, computed from the experimental behavior of $\eta = \eta(c,[NaCl])$.

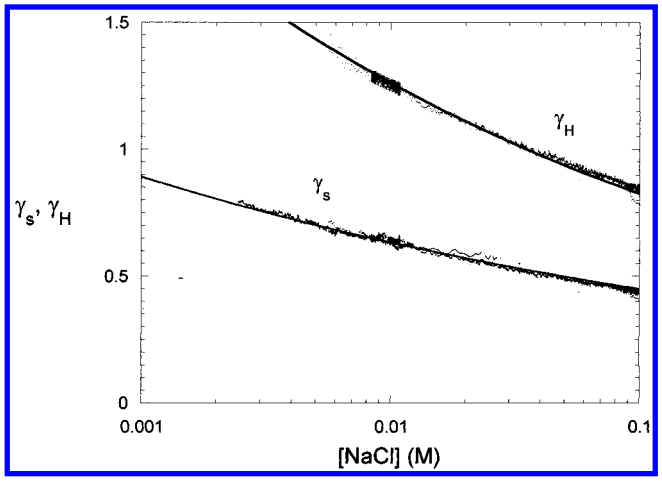

Figure 10. γ_H obtained from combining $[\eta]$ and A_2 as explained in the text. Also shown is γ_s, obtained from combining $\langle S^2\rangle_z$ and A_2. The inset shows the ratio $R_H/\langle S^2\rangle^{1/2}$, obtained by combining γ_H and γ_s.

where the relative viscosity η_{rel} is given by the usual form

$$\eta_{rel} = \frac{\eta}{\eta_0} - 1 \tag{33}$$

Figure 9 shows isoviscous curves for HA, for different values of η_{rel}.

Now, the relationship between the electrostatic contributions and the steric contributions to the parameters $[\eta]$, A_2, A_3, and $\langle S^2\rangle^{1/2}_z$ can be investigated. $[\eta]$ measures hydrodynamic volume V_H ($=4\pi R_H^3/3$, where R_H is the equivalent hydrodynamic radius of the polymer), according to eq 7.

A_2 for a hard sphere of radius R is given by the well-known expression

$$A_2 = \frac{16\pi R^3 N_A}{3M^2} \tag{34}$$

This is the $q = 0$ limit of the second term in eq 17.

A relation between R_H and R can be given as $R = \gamma_H R_H$, and γ_H can then be evaluated by combining eqs 7 and 34. Figure 10 shows that γ_H decreases monotonically with [NaCl], essentially logarithmically over the range 0.010−0.1 M. This implies that the effective sphere radius R responsible for A_2 increases more rapidly than R_H, suggesting that R represents an electrostatically enhanced sphere of exclusion, that $[\eta]$ is largely insensitive to.

Similarly a relation can be defined such that $R = \gamma_s\langle S^2\rangle^{1/2}$. The result is also shown in Figure 10. It shows the same type of behavior, as the hydrodynamic factor, in that the effective R governing A_2 grows more rapidly than $\langle S^2\rangle^{1/2}$ as [NaCl] decreases. Combining the data on R_g and R_H via the relation $R_H = a\langle S^2\rangle^{1/2}$ yields a value that increases gradually from 0.59 to 0.61. This value is not far from the predicted nondraining value of 0.67. Finally, if $[\eta]$ is plotted vs $\langle S^2\rangle^{1/2}$ (not shown), an approximate power law of 2.6 is found. This is close to the value of 2.43 predicted by Yamakawa and others.[62−64]

A final topic for brief discussion is the contribution of the polyelectrolyte ions to the solution ionic strength [I] (in M), sometimes termed the "self-salt" effect. Often, the contribution to [I] due to the polyelectrolyte's counterions has been approximated as simply the counterion portion to the usual computation of a simple electrolyte ($c_s = 0.5z_c^2$[CI], where [CI] is the molar concentration of the counterion, and z_{ci} the number of elementary charges it bears), omitting the contribution of the polyion charge, according to eq 10.

The raw light-scattering data for the HA concentration ramp at 0.0005 M NaCl in Figure 3 is the first indication that the counterions due to the increasing HA concentration are contributing the ionic strength and hence decreasing A_2 and A_3 as c increases. Constant, positive A_2 and A_3 terms in eq 3 lead to a continued decrease in scattering intensity with c after the maximum is reached, so the fact that a minimum is reached for the 0.0005 M NaCl data suggests that A_2 and/or A_3 have decreased due to the counterion contribution to ionic strength, allowing scattering intensity to rise as c increases further. In the other curves shown in Figure 3, the effect is not seen because the concentration of NaCl to [I] is much higher than the HA counterion contribution. Using the approximate power laws for A_2 and A_3 vs [NaCl], obtained in the regions where the HA counterion contribution to [I] is negligible, allows A_2 to be found as $A_2 = A_2([NaCl] + \beta c)$, and likewise for A_3. Differentiating $I(c,q = 0)$ with respect to c allows a prediction for the minimum in the scattering data for [NaCl] = 0.0005 M to be predicted, with β the free parameter. The value of $\beta = 2.3$ best solves for the experimentally found minimum.

The crossover of η_r in Figure 7 is further evidence of the "self-salt" effect. By using eq 6 for η_r, and the approximate power law dependence for $[\eta]$, obtained in the high [NaCl] regime, where HA counterion contribution to c_s is negligible, together with the value of $k_H = 0.04$ at low [NaCl] leads to a value of $\beta = 3$ (M mL/g) in the expression. The values of β obtained from both the light-scattering and viscosity data are close to but higher than the value of 1.25 M mL/g that is obtained if one assumes only the counterions of HA contribute to [I].

Another effect that has been often traced to the polyelectrolyte's counterion contribution to [I] is the electroviscous effect. The inset to Figure 8 shows the electroviscous effect for HA, at 0.0005 M NaCl. A maximum in η_r is reached as c decreases, after which η_r decreases with a further decrease in c, as for a neutral polymer. Several models have been advanced for explaining the maximum for semiflexible polyelectrolytes, most being based on the argument that as the polyelectrolyte solution is diluted with a fixed, low salt concen-

tration stock solution, [I] of the solution decreases, because of the dilution of the polyelectrolyte's counterions. There are then different models as to how the decreasing ionic strength causes the maximum: e.g., by simply swelling the coil dimensions and increasing $[\eta]$[65] or by increasing the hydrodynamic volume causing the second-order interaction terms in eq 6 to a greater degree than volume per polyelectrolyte chain decreases.[66]

Summary

An automatic dilution technique is used to obtain a continuous record of how light-scattering and viscosity behavior vary for a linear polyelectrolyte, HA, as ionic strength varies at fixed polyelectrolyte concentration, or vice versa. The record of this behavior allows continuous data on A_2, A_3, $\langle S^2\rangle_z$, and η_r to be simultaneously obtained. The effects of strong interparticle correlations are also observable at very low values of [NaCl], via the behavior of the slope of $Kc/I(q,c)$ vs q^2, which becomes dominated by interparticle effects, and even becomes negative at sufficiently low [NaCl]. The behavior of $\langle S^2\rangle$ and A_2 is fairly well described by a combination of EPL and EEV theories proposed earlier, which require no adjustable parameters. The EEV effects are shown to be predominant. The data allow the relationship between electrostatic and steric effects to be explored via the values of $\langle S^2\rangle^{1/2}$, A_2, A_3, and $[\eta]$. A_3 is proportional to A_2^2 over the range of 0.001−0.2 M [NaCl]. This is predicted by even a simple equivalent hard sphere model for the electrostatically enhanced virial coefficients, although the proportionality factor is about 1/10 the value obtained for hard spheres. Values on the order of 0.2−0.5 times the hard sphere proportionality are typically found for neutral polymers. The fact that the equivalent hard sphere radius increases with decreasing [NaCl] more rapidly than the electrostatically enhanced $\langle S^2\rangle^{1/2}$ indicates that the equivalent hard sphere radius for A_2 and A_3 become dominated by an effective electrostatic radius, measurably in excess of $\langle S^2\rangle^{1/2}$. In the very low [NaCl] regime, the effects of the polyelectrolyte's own counterions to solution ionic strength is seen in the electroviscous effect, the overall η_r vs c data, and in the minimum in scattering intensity vs c seen for the 0.0005 M NaCl experiment of Figure 3.

The behavior of the polyelectrolyte conformational and interaction parameters is followed at a level of detail previously unobtainable by manual gathering of individual data points. It is hoped that the ACM technique will prove to be a general and useful technique for polyelectrolyte research.

Acknowledgment. Support from NSF CTS 0124006 is gratefully acknowledged.

References and Notes

(1) Nierlich, M.; Boue, F.; Lapp, A.; Oberthur, R.; *J. Phys. (Paris)* **1983**, *44*, 87.
(2) Nierlich, M.; Williams, C. E.; Boue, F.; Cotton, J. P.; Daoud, M.; Farnoux, B.; Jannink, G.; Picot, C.; Moan, M.; Wolff, C.; Rinaudo, M.; de Gennes, P. G. *J. Phys. (Paris)* **1979**, *40*, 701.
(3) Nallet, F.; Jannink, G.; Hayter, J.; Oberthur, R.; Picot, C. *J. Phys. (Paris)* **1983**, *44*, 87.
(4) Wang, L.; Bloomfield, V. A. *Macromolecules* **1991**, *24*, 5791.
(5) Drifford, M.; Dalbiez, J. P. *J. Phys. Chem.* **1984**, *88*, 5368.
(6) Li, X.; Reed, W. F. *J. Chem. Phys.* **1991**, *94*, 4568.
(7) Maier, E. G.; Krause, R.; Deggelmann, M.; Hanegbuchle, M.; Weber, R.; Fraden, S. *Macromolecules* **1992**, *25*, 1125.
(8) Forster, S.; Schmidt, M.; Antonietti, M. *Polymer* **1990**, *31*, 781.
(9) Morfin, I.; Reed, W.; Rinaudo, M.; Borsali, R. *J. Phys. (Paris)* **1994**, *4*, 1001.
(10) Reed, W. F. *J. Chem. Phys.* **1994**, *100*, 7825.
(11) Fuoss, R. M.; Strauss, V. P. *J. Polym. Sci.* **1948**, *3*, 602.
(12) Basu, S. *Nature (London)* **1951**, *168*, 341.
(13) Rinaudo, M.; Milas, M.; Jouon, M.; Borsali, R. *Polymer* **1993**, *34*, 3710.
(14) Rau, D. C.; Lee, B.; Parsegian, V. A. *Proc. Natl. Acad. Sci. U.S.A.* **1984**, *81*, 2621.
(15) Podgornik, R.; Rau, D. C.; Parsegian, V. A. *Macromolecules* **1989**, *22*, 1780.
(16) Rau, D. C.; Parsegian, V. A. *Science* **1990**, *249*, 1278.
(17) Peitzsch, R. M.; Reed, W. F. *Biopolymers* **1992**, *32*, 219.
(18) Forster, S.; Schmidt, M. *Adv. Polym. Sci.* **1995**, *120*, 53.
(19) Yamakawa, H. *Modern Theory of Polymer Solutions*; Harper & Row: New York, 1971.
(20) Ghosh, S.; Li, X.; Reed, C. E.; Reed, W. F. *Biopolymers* **1990**, *30*, 1101.
(21) Michel, R. C.; Reed W. F. *Biopolymers* **2000**, *53*, 19.
(22) Lin, S. C.; Li, W. I.; Schurr, J. M. *Biopolymers* **1978**, *17*, 1041.
(23) Drifford, M.; Dalbiez, J. P. *Biopolymers* **1985**, *24*, 1501.
(24) Ghosh, S.; Peitzsch, R. M.; Reed, W. F. *Biopolymers* **1992**, *32*, 1105.
(25) Smits, R. G.; Kuil, M. E.; Mandel, M. *Macromolecules* **1984**, *27*, 5599.
(26) Norwood, D. P.; Benmouna, M.; Reed, W. F. *Macromolecules* **1996**, *29*, 4293.
(27) Manning, G. *J. Chem. Phys.* **1969**, *51*, 924.
(28) Villetti, M.; Borsali, R.; Diat, O.; Soldi, V.; Fukada, K. *Macromolecules* **2000**, *33*, 9418.
(29) Streliztki, R.; Reed, W. F. *J. App. Polym. Sci.* **1999**, *73*, 2359.
(30) Norwood, D. P.; Reed, W. F. *Int. J. Polym. Anal. Charact.* **1997**, *4*, 99.
(31) Sorci, G. A.; Reed, W. F. *Langmuir* **2002**, *18*, 353.
(32) Zimm, B. H. *J. Chem. Phys.* **1948**, *16*, 1093.
(33) Peitzsch, R. M.; Burt, M. J.; Reed, W. F. *Macromolecules* **1992**, *25*, 806.
(34) Reed, C. E.; Li, X.; Reed, W. F. *Biopolymers* **1989**, *28*, 1981.
(35) Casassa, E. F.; Eisenberg, H. *J. Phys. Chem.* **1960**, *64*, 753.
(36) Ooi, T. *J. Polym. Sci.* **1958**, *28*, 459.
(37) Huggins, M. L. *J. Am. Chem. Soc.* **1942**, *64*, 2716.
(38) Bohdanecky, M.; Kovar, J. In *Viscosity of Polymer Solutions*; Jenkins, A. D., Ed.; Polymer Science Library 2; Elsevier, New York, 1982.
(39) Brandrup, J., Immergut, E. H.; Eds. *Polymer Handbook*, 3rd ed.; John Wiley & Sons: New York, 1989.
(40) Nordmeier, E. *Polym. J.* **1995**, *1*, 25.
(41) Scatchard, G.; Batchelder, A. C.; Brown, A.; Zosa, M. *J. Am. Chem. Soc.* **1946**, *68*, 2610.
(42) Hansen, J. P.; McDonald, I. R. *The Theory of Simple Liquids*; Academic Press: New York, 1986.
(43) Nakamura, Y.; Norisuye, T.; Teramoto, A. *J. Polym. Sci., Part B: Polym. Phys.* **1991**, *29*, 153.
(44) Kniewske, R.; Kulicke, W. M. *Makromol. Chem.* **1983**, *184*, 2173.
(45) Appelt, B.; Meyerhoff, G. *Macromolecules* **1980**, *13*, 657.
(46) Bruns, W. *Macromolecules* **1997**, *30*, 4429.
(47) Benoit, H. *J. Polym. Sci.* **1953**, *11*, 507.
(48) Benmouna, M.; Weill, G.; Benoit, H.; Akcasu, Z. *J. Phys. (Paris)* **1982**, *43*, 1679.
(49) Hayter, J. B.; Penfold, J. *Mol. Phys.* **1981**, *42*, 109.
(50) Landau, L. D.; Lifschitz, E. M. In *Statistical Physics*, 3rd ed.; Pergamon Press: Oxford, England, 1963; Part 1, Chapter 12.
(51) Tricot, M. *Macromolecules* **1984**, *17*, 1698.
(52) Fisher, L. W.; Sochor, A. R.; Tan, J. S. *Macromolecules* **1977**, *10*, 955.
(53) Reed, W. F.; Ghosh, S.; Hedjahdi, G.; Francois, J. *Macromolecules* **1991**, *24*, 6189.
(54) Reed, C. E.; Reed, W. F. *J. Chem. Phys.* **1991**, *94*, 8479.
(55) Reed, W. F. In *Macroion Characterization*; Schmitz, K., Ed.; American Chemical Society, Washington, DC, 1994.
(56) Odijk, T. *Polym. Sci. Phys. Ed.* **1977**, *15*, 477.
(57) Skolnick, J.; Fixman, M. *Macromolecules* **1977**, *10*, 9444.
(58) Gupta, S. K.; Forsman, W. C. *Macromolecules* **1972**, *5*, 779.
(59) Beer, M.; Schmidt, M.; Muthukumar, M. *Macromolecules* **1997**, *30*, 8375.
(60) Muthukumar, M. *J. Chem. Phys.* **1987**, *86*, 7230.
(61) Muthukumar, M. *J. Chem. Phys.* **1996**, *105*, 5183.
(62) Yamakawa, H.; Kurata, M. *J. Phys. Soc. Jpn.* **1958**, *13*, 94.
(63) Kurata, M.; Yamakawa, H. *J. Chem. Phys.* **1958**, *29*, 311.
(64) Weill, G.; des Cloizeaux, J. *J. Phys. (Orsay, Fr.)* **1979**, *40*, 99.
(65) Hodgson, D. F.; Amis, E. J. *J. Chem. Phys.* **1991**, *94*, 4581.
(66) Reed, W. F. *J. Chem. Phys.* **1994**, *101*, 2515.

MA012103N